

Multi-temporal Synthetic Aperture Radar Metrics Applied to Map Open Water Bodies

Maurizio Santoro, *Member, IEEE*, and Urs Wegmüller, *Senior Member, IEEE*

Abstract—Multi-temporal synthetic aperture radar (SAR) metrics are assessed to map open water bodies. High temporal variability and low minimum value in a time series of Envisat Advanced SAR (ASAR) Wide Swath Mode (WSM) backscatter measurements characterize open water bodies with respect to other land cover types. Confusion occurs in the case of steep terrain (slope angle $> 10^\circ$), less than 10 backscatter observations and for mixed pixels with a water fraction. The behavior of the two SAR multi-temporal metrics is consistent at six study areas in Europe and Central Siberia. A simple thresholding algorithm applied to the multi-temporal SAR metrics to map open water bodies performs with overall accuracies above 90% in the case of pure pixels of water or land. The accuracy decreases when mixed pixels are accounted for in the reference dataset and for increasing land fraction in the reference samples. An overall accuracy of approximately 80% was obtained for a 50% threshold of the water fraction. Omissions of water areas occur mostly along shorelines. Specific conditions of the land surface can distort the minimum, causing commission in the water class. The use of a low order rank or percentile instead of the lowest backscatter value can reduce such commission error.

Index Terms—Envisat ASAR, minimum backscatter, SAR backscatter, temporal variability, water bodies, wide swath mode.

I. INTRODUCTION

SPACEBORNE Synthetic Aperture Radar (SAR) data are available from a number of satellites operating at different wavelengths, with multi-mode image configurations and are operated with different acquisition strategies. Typically, the acquisition of high resolution SAR systems (1–20 m) targets specific areas. Sensors with acquisition modes at moderate resolution (100–1,000 m) are instead operated to acquire data on a global scale in a repeated manner. In view of generating estimates of a land surface parameter for large areas, moderate resolution image data products become the only practical alternative if a mapping solution based on SAR data is explored. The availability of repeated acquisitions is of advantage since multi-temporal observations allow reduction of speckle noise [1], detection of trends in land surface parameters such as soil moisture [2], wetlands [3]–[5], cropland [6] and water bodies [7]–[9]. In addition, multi-temporal data allow the generation of additional

parameters, herewith referred to as multi-temporal metrics, with acknowledged potential in thematic mapping [10][11].

The major limitation of single SAR backscatter images to map water bodies relies in the dependence of the backscattered signal upon the surface conditions of the water body. Thresholding approaches or supervised approaches applied to a single image were sufficient to detect and delineate lakes and rivers in C- and X-band co-polarized data as long as the backscatter was overall low with respect to other land surfaces [12]–[17]. Several authors reported false detections of water as land in the case of rugged water surface [12]–[15], which could be compensated for to a certain extent by using active contour methods [12], [18]. The generation of a global Water Indication Mask (WAM) from X-band TanDEM-X/TerraSAR-X image pairs [15], [18], [19] profits from a combination of classifications based on SAR amplitude and interferometric SAR coherence using individual threshold-based approaches on each observable [19]. Classification accuracy reported in terms of correctness and completeness was between 51% and 72%, and 60% and 81%, respectively, for three latitudinal transects. Slightly higher accuracy was obtained when using coherence data only [19].

Multi-temporal observations were used to understand and quantify dynamics of water bodies [5], [8], [9], [13]; a general conclusion was that the temporal sampling even in the case of very frequent observations as in the case of Envisat ASAR ScanSAR images was not optimal to track dynamics in a sufficiently detailed manner. Multi-temporal observations furthermore revealed changes of the SAR backscatter over lakes and rivers covered with ice [7], [20]. For bottom-fast ice, low backscatter was observed; in the case of liquid water under the ice, the SAR backscatter level depended on the composition of the ice layer [21]–[24].

The objective of this paper is to investigate the properties of metrics derived from multi-temporal SAR data and demonstrate their usefulness in the context of land surface characterization with particular regard to the detection of open water bodies. Ultimately, the goal was to assess the potential of moderate resolution SAR data to complement classification of water bodies in global land cover products [25]. To this scope, we aimed at setting up and validating a water body mapping algorithm that could be straightforward and robust at the same time.

The SAR dataset consisted of images of the radar backscattered intensity acquired by the Envisat Advanced SAR (ASAR) instrument. To assess the consistency of the multi-temporal metrics and the robustness of the water body mapping approach from the SAR data here considered, investigations were undertaken at several study areas characterized by different typologies of land cover and water bodies, terrain

Manuscript received May 03, 2013; revised July 04, 2013; accepted October 29, 2013. This work was supported by the European Space Agency within the Climate Change Initiative Land Cover (CCI-LC) project.

M. Santoro and U. Wegmüller are with GAMMA Remote Sensing AG, CH-3073 Gümligen, Switzerland (e-mail: santoro@gamma-rs.ch; wegmueller@gamma-rs.ch).

Color versions of one or more of the figures in this paper are available online at <http://ieeexplore.ieee.org>.

Digital Object Identifier 10.1109/JSTARS.2013.2289301

TABLE I
LIST OF STUDY AREAS. CORNER COORDINATES REFER TO TOP-LEFT (TL) AND BOTTOM-RIGHT (BR)
COORDINATES EXPRESSED IN THE FORM OF LATITUDE AND LONGITUDE

Area	Corner coordinates (Lat./Long.)	Area (10^6 km^2)	Land cover features
Andalusia, Spain	TL=(41°N, -8°E) BR=(36°N, -1°E)	3.39	Reservoirs and rivers, cities, cropland
Central Siberia	TL=(60°N, 91°E) BR=(54°N, 99°E)	3.25	Rivers, forest, pasture
Netherlands	TL=(54°N, 3°E) BR=(50°N, 8°E)	1.53	Rivers, lakes, agriculture, urban
Poland & Belarus	TL=(56°N, 17°E) BR=(52°N, 25°E)	2.34	Lakes, rivers, wetlands, forest, agriculture
Switzerland	TL=(48°N, 5°E) BR=(45°N, 11°E)	1.54	Lakes, rivers, snow/ice, cities, cropland
Västerbotten, Sweden	TL=(67°N, 14°E) BR=(63°N, 22°E)	1.68	Lakes, forest, peat bogs

conditions and seasonality. Section II provides an overview of the study areas. Section III describes the SAR datasets and the reference datasets. Section IV presents the signature analysis of multi-temporal metrics for different land cover classes. Section V describes the approach developed to map water bodies using the multi-temporal SAR metrics found to be most suitable for this application. Classification results and agreement statistics with respect to the reference datasets are discussed in Section VI. Finally, a set of conclusions are presented in Section VII.

II. STUDY AREAS

Multiple sites were considered in order to obtain broad understanding of SAR metrics potentially suitable for mapping water bodies and to come up with a robust mapping algorithm, capable to withstand effects of seasonal conditions on the SAR backscatter and different land cover composition. Six study areas were selected (see Table I) following these requirements:

- (i) diverse landscape in terms of land cover, water bodies and topography;
- (ii) diverse seasonal and environmental conditions;
- (iii) availability of large number of SAR backscatter measurements within a one-year period;
- (iv) availability of reliable datasets to be used as reference.

While this selection captured a wide diversity of land cover types, we did not explicitly consider areas characterized by temporal dynamics (e.g., due to inundation) because beyond this first evaluation of multi-temporal SAR metrics in water body characterization. The size of the study areas ranged between $1.53 \cdot 10^6 \text{ km}^2$ and $3.39 \cdot 10^6 \text{ km}^2$ (Table I). In total, detection of water bodies with multitemporal SAR metrics was tested for more than $13 \cdot 10^6 \text{ km}^2$.

III. DATASETS

A. SAR Dataset

The SAR dataset consisted of images acquired by Envisat ASAR in the Wide Swath Mode (WSM). The ASAR instrument operated at C-band (wavelength of 5.7 cm) with a multi-mode configuration [26]. Because of the large swath of the WSM mode (approximately 400 km), any point on the ground could be observed several times throughout the repeat-pass interval of the satellite (35 days between January 2002 and October 2010,

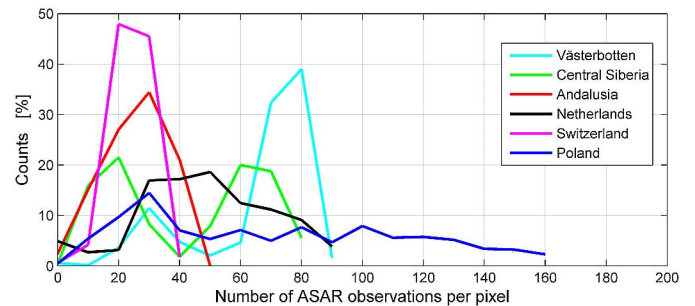


Fig. 1. Histograms of number of ASAR observations per pixel for each study area. Number of observations have been binned in classes of 10 observations each.

then 30 days until April 2012). A WSM image was characterized by look angles spanning between 18° (near range) and 42° (far range). The data were acquired in single-polarization mode, either Horizontal-Horizontal (HH) or Vertical-Vertical (VV).

For this study, a one-year dataset of all Envisat ASAR WSM images over each of the study areas was considered. It was assumed that the number of backscatter observations collected within one year would have been sufficient to provide reliable multi-temporal SAR metrics while there would have been only minor large scale changes of the landscape. To avoid large differences in time with the date of the reference datasets (Section III-B), the SAR dataset consisted of all images acquired in 2005. Table II presents an overview of the number of images covering each study area. Images were available from ascending and descending orbits and were acquired mostly in VV polarization. Fig. 1 shows the histogram of the number of ASAR observations per pixel. For each site, the smallest number of observations were located in correspondence of the edges.

The ASAR WSM data consisted of images of the backscattered intensity (Level 1P products) with a pixel size of $75 \text{ m} \times 75 \text{ m}$, whereas the spatial resolution is approximately 120 m both in range and in azimuth direction [27]. The SAR images were first calibrated using factors provided by ESA in the image data file. A buffer zone along the perimeter of an image was removed because of occasional processing artifacts. Multi-looking, i.e., spatial averaging, in a 4×4 window was applied to obtain images with a pixel size of $300 \text{ m} \times 300 \text{ m}$. This resolution was selected to be in line with the resolution of global land cover mapping efforts [25], [28]. However, a 2×2

TABLE II
NUMBER OF ENVISAT ASAR WIDE SWATH IMAGES FOR EACH OF THE STUDY AREAS. EACH IMAGE CORRESPONDS TO A 400-KM-WIDE IMAGE TAILORED IN LENGTH BY ESA TO COVER THE STUDY AREA. FOR THE NUMBER OF OBSERVATIONS PER PIXEL, REFER TO FIG. 1.

Study area	Number of ASAR images (HH / VV / Total)
Andalusia	5 / 80 / 85
Central Siberia	1 / 70 / 71
Netherlands	11 / 84 / 95
Poland	0 / 160 / 160
Switzerland	1 / 52 / 53
Västerbotten	37 / 118 / 155
TOTAL	55 / 564 / 619

multi-looked version of the original dataset with an output pixel size of $150\text{ m} \times 150\text{ m}$ was also generated for the study area of the Netherlands to investigate the impact of spatial resolution on water body mapping.

For each study area, the corresponding SAR images were terrain geocoded [29] to the geographic projection using the 3-arcsec Shuttle Radar Topography Mission (SRTM) Digital Elevation Model [30] south of 60°N or digitized terrain elevation information [31] north of 60°N . A look-up table describing the transformation between the radar and the map geometry was generated based on orbital parameters and the DEM. To correct for geolocation errors due to errors of orbital parameters or the SAR image metadata, a refinement of the lookup table was applied. The refinement consisted of estimating the offset between the SAR backscatter image to be geocoded and a reference image for the output geometry [32]. The reference image was typically a SAR backscatter image simulated from the DEM. Because of the predominantly flat terrain within the study areas of the Netherlands and Poland, the latter image did not present any feature that would match with the SAR backscatter image. Here, the reference consisted of a mosaic of Landsat images obtained through the Global Land Cover Facility (GLCF, <http://glcf.umd.edu>), resampled to the pixel size of the SAR data.

The registration error of the SAR images with respect to the reference datasets was less than $1/3\text{rd}$ of the pixel size. The SAR images with 300 m pixel size were geocoded to $1/360\text{th}$ of a degree, in accordance with the GlobCover product [25]. SAR images with a pixel size of 150 m were geocoded to corresponding pixel sizes in degrees, i.e., $1/720\text{th}$ of a degree.

The co-registered SAR images were filtered with a multi-temporal approach to decrease speckle noise [1]. The filtered images were obtained from the original dataset by means of a linear combination with weights corresponding to the local spatial average of the individual (unfiltered) intensity channels. Over textured terrain, however, spatially adaptive filters allow better estimates of the radar cross section; hence, it was chosen to define the weights starting from a speckle-reduced image obtained with the GAMMA MAP filter [33] rather than from the original unfiltered image. The advantage of the multi-temporal approach compared to a spatial filter is preservation of spatial resolution.

To quantify the uncertainty of the backscatter measurements, the Equivalent Number of Looks (ENL) [34] was estimated. The ENL was computed in polygons that visually showed small spatial variability of the backscatter. To understand the impact of the number of observations available per pixel on the ENL estimates, polygons were located in areas including at least 20 observations of the backscatter. The proportion of pixels with less than 20 backscatter observations was small; such pixels were mostly located at the edge of a study area.

The ENL of Envisat ASAR WSM Level 1P images was reported to be approximately 15 [27]. As a result of multi-looking, the ENL of the backscatter images with a pixel size of 300 m was mostly between 40 and 60 (corresponding to $0.6\text{--}0.7\text{ dB}$ uncertainty of the backscatter). This result is explained by considering that Level 1P data is oversampled by factors close to 2 in range and in azimuth; therefore, multi-looking in a 4×4 window corresponds to averaging over approximately 4 independent looks. After speckle filtering, the ENL was mostly between 130 and 170, corresponding to a backscatter uncertainty of $0.3\text{--}0.4\text{ dB}$. The ENL estimates did not show dependence upon the number of observations per pixel. Based then on the results of the signature analysis (see Section IV), it was reasonable to assume that the backscatter uncertainty would play a minor role in this study.

As a final step, compensation of the SAR backscatter in the case of sloped terrain was applied as described in [35], [36] using an estimate of the pixel area and the local incidence angle.

B. Land Cover Datasets

Two land cover datasets with proven thematic accuracy, geometric precision and reliability were selected to act as reference throughout this study: the CORINE (Coordination of Information on the Environment) land cover dataset [37] and the SRTM Water Bodies Dataset (SWBD) [38].

The CORINE land cover dataset was produced for the large majority of the member states of the European Union with a spatial resolution of 100 m and 250 m for the years 1990, 2000, and 2006 from high-resolution optical imagery. For our work, the 250 m dataset of 2006 (referred to as CLC2006) was considered [39].

The SRTM Water Bodies Dataset (SWBD) is a vector dataset derived from the SRTM data acquired in February 2000. It shows shoreline of water bodies (lakes, rivers and oceans) at the time of acquisition of the radar data [38]. The dataset covers all land masses between 60°N and 60°S with a spatial resolution of 90 m . The time difference between the SRTM and the ASAR dataset (five years) was taken into account by cross-checking the SWBD dataset with Google Earth imagery in the case of large differences between SWBD and the mapping result from the ASAR dataset (e.g. recent water reservoirs).

For the comparison with the SAR datasets and the corresponding water body maps, the CLC2006 and SWBD datasets were transformed to the map geometry and the pixel size of the geocoded SAR data. The CLC2006 land cover was resampled with a nearest neighbor approach. The SWBD dataset was rasterized to the pixel size of the SAR datasets. The CLC2006 and the SWBD datasets complemented each other to cover all study

areas. For study areas where both datasets were available, the agreement in terms of water and land classes was above 90%.

C. Samples Based on Google Earth Imagery

Samples extracted from high-resolution imagery in global image and map viewers such as Google Earth are an alternative approach to generate reference information. In this study, a stratified random sampling approach has been developed to select land and water samples in equal manner. Polygons corresponding to a pixel in the SAR image were overlaid onto Google Earth image and the land cover therein was interpreted. In the case of mixed water/land cover, e.g., in proximity of shorelines, the water cover fraction within the polygon was also estimated. The estimates were reported in intervals of 5%; a value of 1% refers to pixels edging a shoreline but not including any significant portion of water. To limit bias due to the operator, the polygons were revisited after some time and a second estimation of fractional water cover was performed. The estimates of water fraction differed at most by 10% from which we concluded that the estimates of water fraction were sufficiently reliable to be used as reference. The number of reference samples was determined with respect to a minimum required product accuracy and confidence level [40]. To obtain a classification accuracy of at least 85% with a confidence level of 0.05, 93 was the minimum number of samples required. To allow a correct representation of the three possible classes involved in our study (“pure” water, “pure” land and mixed pixels), 279 samples were selected for each study area.

When labeling each sample, the year of the image in Google Earth was taken into account. The majority of the samples were evaluated from high-resolution imagery acquired in 2005 and 2006. Samples for which data were available for 2009 and 2010 only were cross-checked with the CLC2006 or the SWBD datasets. The screening did not reveal any difference between the Google Earth samples and the raster dataset.

IV. SIGNATURE ANALYSIS

The multi-temporal SAR metrics considered in this study were the minimum backscatter (MB) and the temporal variability (TV) of the backscatter defined as the standard deviation of the backscattered intensities in the logarithmic decibel (dB) scale. The use of the dB scale for the latter parameter enhanced the contrast with respect to a standard deviation based on intensities in the linear scale.

Fig. 2 shows the images of TV and MB for the study area of Västerbotten. Inland water bodies and the Gulf of Bothnia in the east of the study area were characterized by the highest TV and lowest MB. To get an understanding for the behavior of TV and MB of water and land surfaces, Fig. 3 shows the time series of the SAR backscatter for three pixels labeled in CLC2006 as water body, arable land and forest, respectively. The continuous variation of the SAR backscatter in time over open water implied the highest TV among the three cases here considered. The TV of arable land was affected by changes of the backscatter during the growing season, located approximately in the middle of the time series. The TV of forest was very low since the backscatter was rather constant in time. The

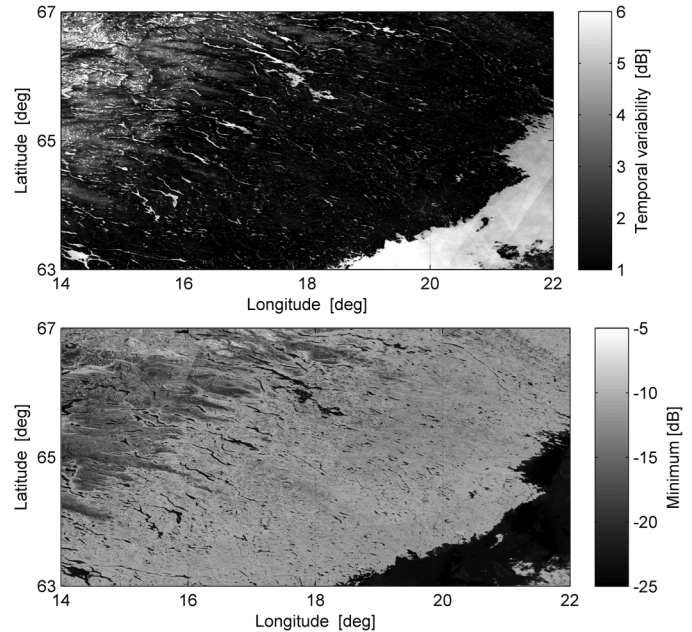


Fig. 2. Images of TV (top) and MB (bottom) for the study area of Västerbotten.

MB was lowest over water because of the repeated occurrence of specular scattering in the forward direction (i.e., calm wind conditions).

In this study, we assumed that the effect of noise in areas of very low backscatter was negligible. The Noise Equivalent Sigma Zero (NESZ) of Envisat ASAR in Wide Swath Mode was between -21 and -26 dB [41]. Such values occurred seldom and only for water areas (see Fig. 3). The effect of NESZ was found to be negligible when the MB was set equal to a low rank parameter of the backscatter histogram rather than to the lowest value.

The different behavior of TV and MB over water and land is further shown by the density plots in Fig. 4 for the study area of the Netherlands and the major four land cover classes therein. Land cover classes were identified using the CLC2006 product. A one-pixel edge-eroded version of the CLC2006 product was used to focus on pure pixels of a certain land cover type.

While the range of values of the individual parameters overlapped, the combination of TV and MB showed a clear separation between the water and the land classes. Water presented high TV and low MB in consequence of the strong variability of the SAR backscatter in time and the very low return under calm conditions resulting in specular reflection in the forward direction, respectively. Other land cover classes were mostly characterized by lower TV and higher MB.

Density plots with respect to the most frequent land cover classes were investigated for all study areas. Water bodies were characterized by values of TV mostly above 2 dB and minimum backscatter below -16 dB. Other land cover classes presented TV values between 1 and 3 dB and minimum backscatter above -15 dB. The wetlands class consisted of inland marshes, peat bogs and salines. Marshes and peat bogs were characterized by a rather constant backscatter in time except for areas affected by seasonal flooding, e.g., Doñana wetlands in the south of Andalusia [4] where the TV was between 2 and 3 dB and the MB

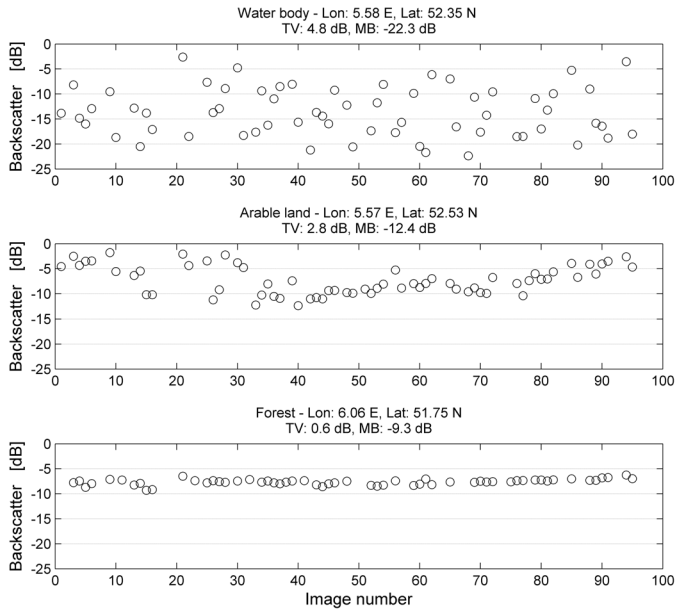


Fig. 3. Time series of SAR backscatter for three pixels labeled in CLC2006 as water body (top), arable land (middle) and forest (bottom), respectively. TV and MB estimates are presented above the corresponding panel. Study area: the Netherlands. Pixel size: $300 \text{ m} \times 300 \text{ m}$.

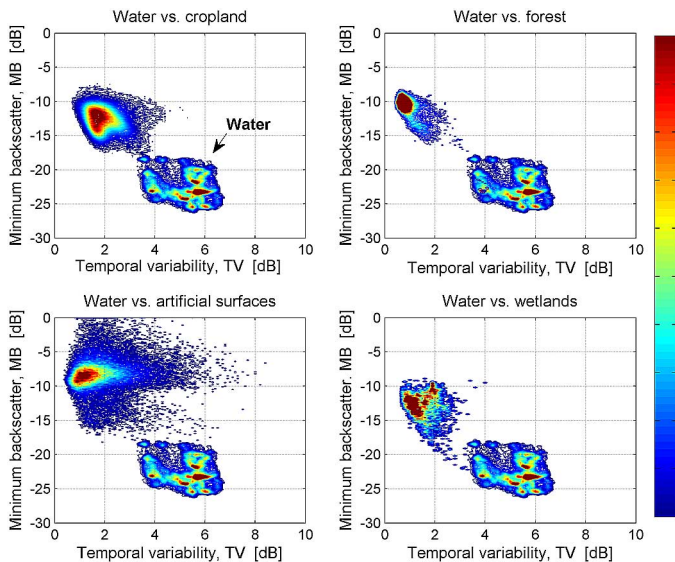


Fig. 4. Density plots of TV and MB for pixels belonging to the water class with respect to major land classes for the study areas of the Netherlands. Increase of density is shown by colors changing from blue to red. The density plot for the water class is shown in each scatterplot for clarity reasons. Pixel size: $300 \text{ m} \times 300 \text{ m}$. Land cover mask: CLC2006.

between -13 and -15 dB, i.e. in between features of permanent land and permanent water surfaces. The MB and TV of salines instead was similar to the observations over open water. In this study, salines were considered as “land” because, in general, they may not be filled with water for a certain period of time.

To quantify the separability between the water class and a land class, the Jeffreys-Matusita (J-M) distance was computed

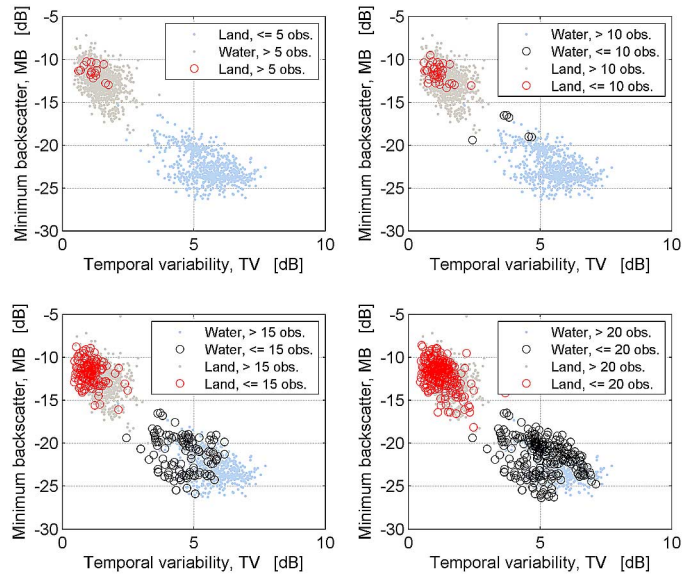


Fig. 5. Scatterplots of TV and MB for water and other land cover classes (pure pixels) and with respect to the number of SAR observations available per pixel. Study area: Andalusia. Pixel size: $300 \text{ m} \times 300 \text{ m}$. Land cover mask: CLC2006 (one-pixel edge eroded).

[42]. A J-M distance close to zero indicates no separability between the classes being compared whereas a distance of 2 indicates total separability. J-M distances were computed for the water class with respect to each of the four major classes in the CLC2006 product (see Fig. 4), for either the TV and the MB. The measured J-M distances were between 1.9 and 2.0 regardless of the metric and the land cover class being compared. These results confirmed very high separability between water and land classes. Nevertheless, there are reasons for which TV and MB over land and water were similar as discussed in the remainder of this section.

A. Number of SAR Backscatter Measurements

Since the TV is defined as a standard deviation, a reliable estimation of the TV requires a large enough number of measurements. Especially over water the TV estimation is affected if the available number of measurements was below 10. Fig. 5 shows four scatterplots of TV and MB for water and other land cover classes, each being characterized by a threshold on number of observations per pixel. The TV and MB of the land pixels were unaffected by the number of observations (red circles vs. grey dots). On the contrary, the TV of water pixels based on less than 10 backscatter measurements was smaller compared to the estimate obtained for water pixels with more backscatter observations (dark circles vs. cyan dots). When considering a higher threshold for the number of observations per pixel (panel for thresholds of 15 and 20 in Fig. 5), the behavior of TV did not differ with respect to pixels characterized by more observations. Although, the interpretation of the different behavior of TV for the threshold of 10 observations is supported by a very small number of pixels and there were not less than 10 observations per pixel at the other study areas, we interpreted the result as a warning that the TV over water could be unreliable if based upon a small number of measurements.

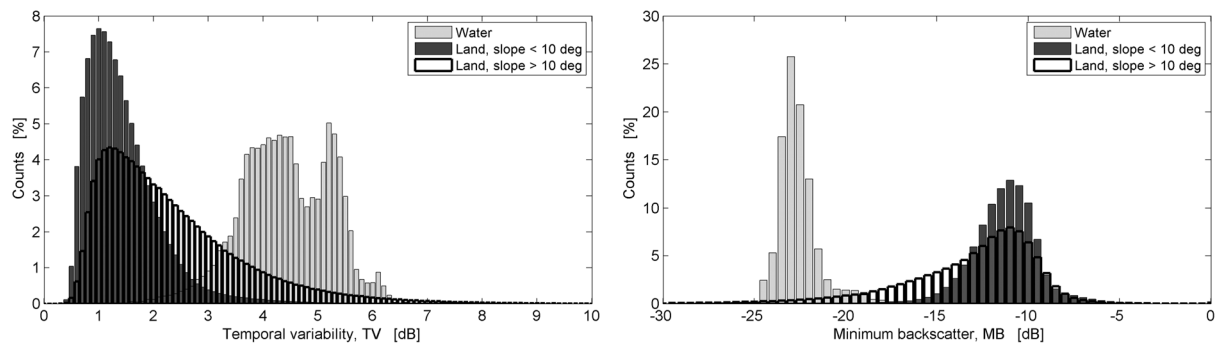


Fig. 6. Histograms of TV (left panel) and MB (right panel) for pixels identified as water, land with slope angle $< 10^\circ$ and land with slope angle $> 10^\circ$ in the Switzerland study area. Pixel size: $300 \text{ m} \times 300 \text{ m}$. Land cover mask: SWBD (one-pixel edge eroded). Slope angle derived from SRTM DEM.

B. Topography

Areas of layover and shadow were identified during SAR processing using information from the DEM, orbital data and look geometry parameters [29] and were masked out from the geocoded SAR images. For other areas on sloped terrain showing modulation of the backscatter after the compensation for pixel area and local incidence angle, we explained such distortions as a consequence of imperfect characterization of slopes in the DEM or orientation-dependent scattering effects [43], [44]. The effect of sloped terrain on TV and MB was investigated by creating histograms for water and land with slope angle either below or above a certain threshold. For a threshold of 10° , we saw the clearest indications on the effect of sloped terrain on the two parameters. The histograms of TV and MB for water and land surfaces with gentle to moderate slopes ($< 10^\circ$) were almost disjoint (Fig. 6). The histograms for land surfaces with steep slopes ($> 10^\circ$) instead committed to more joint parts when compared with the histograms of land surfaces with slopes $< 10^\circ$.

C. Mixed Pixels

The signatures of TV and MB were ambiguous in the case of pixels located along shore- and coastlines with a certain water fraction, i.e., mixed pixels. Fig. 7 shows a scatterplot of TV and MB for pure water (cyan dots), pure land (red dots) and mixed pixels (black circles) in the case of the study area of Andalusia. The values of the two parameters for mixed pixels were located between the clusters of values characteristic of pure water and pure land. The effect of water fraction on TV and MB is further shown in Fig. 8. For a water fraction of 0% (i.e., pure land) or 100% (i.e., pure water), the ranges of values of the two parameter were disjoint. For increasing water fraction, the TV increased whereas the MB decreased with an almost linear trend. For a given water fraction, both parameters presented certain variability, which could be explained as a consequence of the type of scatterers within the fraction of land surface inside the area covered by the pixel. TV was lower when the land part of the pixel consisted of forest rather than cropland and bare soil; similarly, the MB was higher. For mixed pixels with a small fraction of the area corresponding to a single strong scatterer over land (e.g., from infrastructures), the TV was low and the MB was high in consequence of the dominance of this strong and temporally stable scatterer.

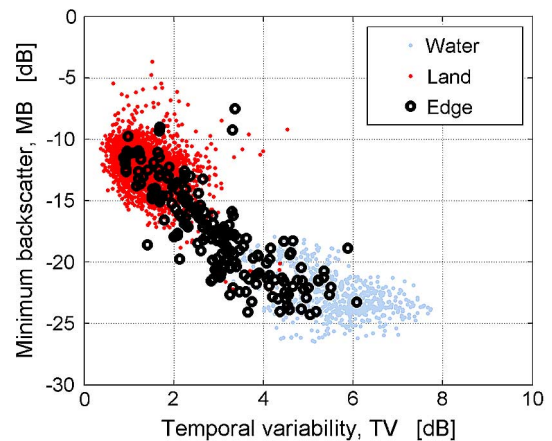


Fig. 7. Scatterplots of TV and MB for pure water, pure land and mixed pixels. Study area: Andalusia. Pixel size: $300 \text{ m} \times 300 \text{ m}$. Land cover mask: SWBD.

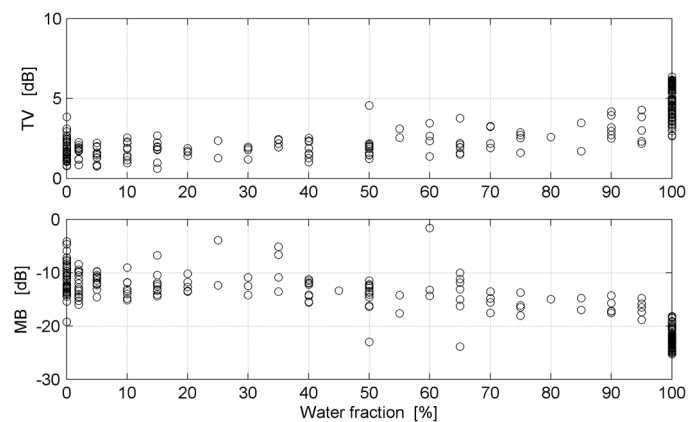


Fig. 8. TV (top) and MB (bottom) with respect to water fraction for the study area of the Netherlands. Pixel size: $300 \text{ m} \times 300 \text{ m}$. Number of samples: 279.

D. Conditions of the Land Cover

Special land cover conditions that occur for a limited time, such as wet snow, flooding of a field etc. [45], can have a strong influence on the backscatter and, consequently, on the multi-temporal SAR metrics. Herewith, we focus on two conditions that occurred at several study areas.

In the case of wet snow, the strong absorption of the microwaves causes very low backscatter, which in turn increases the temporal variability of the backscatter and produces a very

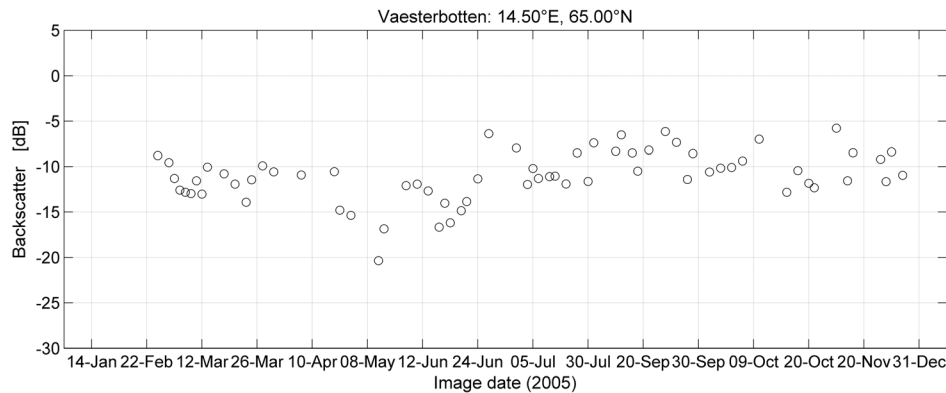


Fig. 9. Time series of ASAR WSM backscatter for a pixel over barren ground within the study area of Västerbotten. Pixel size: $300\text{ m} \times 300\text{ m}$. Thawing conditions of snow cover registered on 08 May. $TV = 2.7\text{ dB}$ and $MB = -20.3\text{ dB}$.

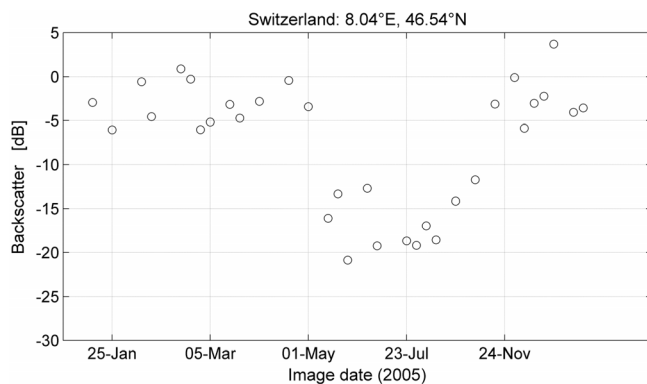


Fig. 10. Time series of ASAR WSM backscatter for a pixel on a glacier within the study area of Switzerland. $TV = 7\text{ dB}$, $MB = -20.8\text{ dB}$. Pixel size: $300\text{ m} \times 300\text{ m}$.

low MB. A first example is shown in Fig. 9 for a time series of backscatter measurements over barren ground. The backscatter dropped on 08-May when weather data reported snow cover and indicated thawing conditions. The TV and the MB for the backscatter time series were 2.7 dB and -20.3 dB , thus falling within the range of values typical of water (see Fig. 4). Any other measurement of the backscatter was above -16 dB whereas the TV was 2.5 dB when the observation of 08 May had been excluded from the time series. The multi-temporal SAR metrics were therefore in the range of values obtained for land surfaces. A second example is shown in Fig. 10 for a time series of backscatter measurements over a glacier. The backscatter was low during late spring and summer (from May until September) because of the wet conditions of the snow cover. The TV and the MB were 7 dB and -20.8 dB . Disregarding data acquired under wet snow conditions, the TV and the MB (2.5 dB and -6.0 dB , respectively) were within the range of values of a land surface.

Depending on the type of crop, the polarization of the microwave and cultivation practice, there can be substantial absorption in the vegetation layer, leading to low minimum backscatter estimates very close to the level observed for water. This issue could be observed at the study areas of Andalusia, the Netherlands, Poland, and Central Siberia. During the summer months, the backscatter of cropland decreased and reached a

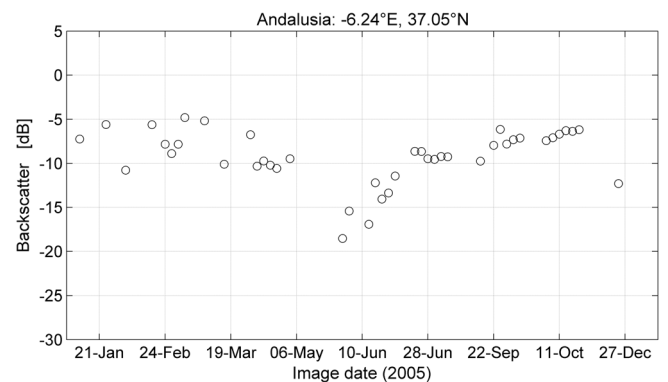


Fig. 11. Time series of ASAR WSM backscatter for a pixel over a rice field at the study area of Andalusia. Pixel size: $300\text{ m} \times 300\text{ m}$.

minimum and then increased during fall until the level before summer. For rice fields, temporary flooding caused sudden decrease of the backscatter, which then increased steadily until harvest (Fig. 11). The consequence was very low minimum backscatter and very large temporal variability (above 4 dB).

E. Using Multiple Orbital Tracks

In the case of a multi-temporal dataset including observations from multiple orbital tracks, the TV and MB are influenced by the different look angles. Discussing look angle dependence of the SAR backscatter for different scattering objects is beyond the scope of this paper. Here, we focus on a comparison between single- and multi-track TV and MB values to understand the impact of look angle on the two parameters. This investigation required that for several tracks, a certain number of backscatter measurements were available to be able to limit bias and uncertainties in the track-wise estimation of TV and MB. Because of the 35-day repeat-pass cycle of Envisat, the maximum number of observations per track in one year was 11. A relatively large number of observations (i.e., more than 5) for several tracks were available only for the Poland study area. Fig. 12 shows an example of track-wise TV and MB for water and cropland. Among the land classes in the study area, cropland presented the largest variability of backscatter. Despite this variability, the single-track TV was always smaller than the corresponding value of water; similarly, the MB was always higher

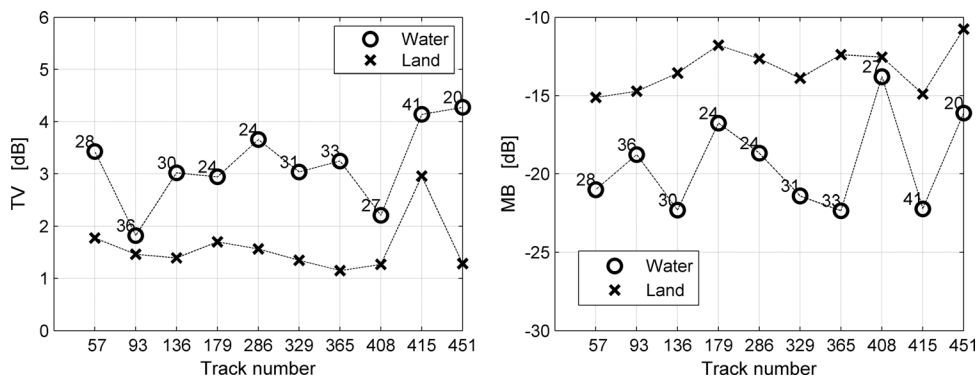


Fig. 12. Single-track TV and MB for two pixels located in areas labeled in the CLC2006 dataset as water and land (cropland), respectively. For each satellite track, the corresponding incidence angle in degrees at the location of the pixel is displayed next to the metric of the water pixel.

for land than for water. Fig. 12 also shows that TV and MB were not much affected by the look angle, here expressed in the form of the local incidence angle to be more precise. The multi-track TV was equal to 4.4 dB (water) and 1.7 dB (land), only slightly higher than the single-track values. The MB was equal to -22.3 dB (water) and -15.1 dB (land), equal to the absolute minimum over all tracks.

In general, TV and MB derived from a multi-track dataset of observations appeared as slightly enhanced with respect to the single-track case. Although, the two parameters can be considered being affected primarily by a temporal component, both also include a geometric component. Our interpretation applies to the land cover types in the six study areas. In polar and desert regions, the backscatter from volumes (snow, ice, or sand layers) or rugged terrain differs depending on the look angle [46], [47] thus introducing a more relevant geometric component in the estimation of TV and MB.

F. Summary

The outcome of the signature analysis is summarized below and served to set up a water body mapping algorithm based on multi-temporal SAR parameters.

1. TV and MB are sufficient for separating water and land surfaces in the case of pure pixels.
2. Water bodies and land surfaces present almost the same signatures regardless if the SAR datasets consists of multi-angle or single-track observations.
3. Mixed pixels might be assigned to one or the other class depending on water fraction and, to a certain extent, on the scattering objects on land.
4. Topographic information in form of slope angle needs to be accounted for to avoid false detections of land as water.
5. The SAR metrics are ambiguous in the case of a small number of backscatter measurements.
6. The definition of MB should rely on a low order rank of the backscatter histogram rather than on the absolute minimum backscatter to avoid that specific events within the time span of the backscatter measurements distort the metric.
7. The impact of polarization on the signatures of TV and MB could not be assessed because the large majority of the ASAR images were acquired in VV-polarization. The only area covered by a number of HH-polarized images sufficient to derive

reliable estimates of TV and MB was the Gulf of Bothnia in the east of the Västerbotten study area. Here, the polarization-specific TV and MB values did not present any difference also when compared to the corresponding values obtained disregarding the polarization. It is, however, necessary to investigate this aspect taking into account that current and future SAR missions will acquire multi-temporal observations either in dual- or in full polarization.

V. WATER BODY CLASSIFICATION METHODOLOGY

The scatterplots of TV and MB of land and water showed symmetry of TV and MB for land and water with respect to a diagonal line represented by a linear equation of increasing MB for increasing TV. A simple thresholding rule in the feature space of TV and MB seemed to be sufficient to map water and land. In this study, we defined the thresholding rule as the diagonal line that was at equal distance from pre-defined clusters of “pure” land and “pure” water in the case of the study area of the Netherlands. The training dataset consisted of 10% of the pixels belonging to each of the two classes according to the CLC2006 dataset.

Equation (1) corresponds to the diagonal line representing the threshold in the feature space of TV and MB:

$$y = 3.5x - 28 \quad (1)$$

Here, x represents the TV in dB and y the MB in dB. This thresholding rule was found to yield a very good separation between pure land and pure water for the Netherlands (Fig. 13) and for all other study areas as well. The observations of TV and MB of mixed pixels were instead crossed by the diagonal line. Ultimately, we preferred setting up a simple classification approach to understand the potential of the TV and MB to separate water and land rather than proceeding with a more complex algorithm already at the beginning of our classification exercise.

The signature analysis furthermore revealed that TV below 1.5 dB and MB above -16 dB are not realistic for water (see Fig. 4). Combining the three thresholding corresponded to defining two portions of the feature space associated to water and land respectively (Fig. 13).

To avoid false detections of land as water in the case of steep topography, pixels characterized by a slopes steeper than 10°

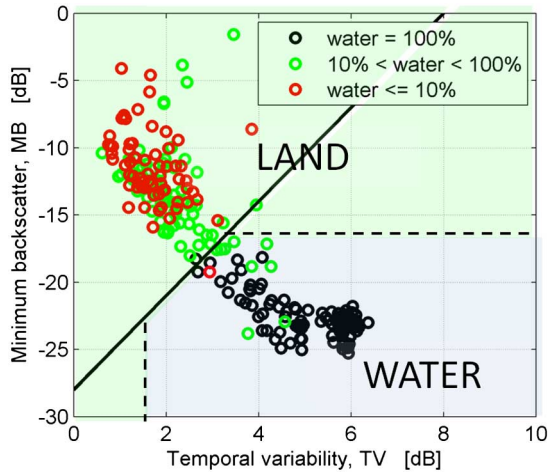


Fig. 13. Illustration of the water body mapping algorithm. Decision rules are represented by the black diagonal line and the two dashed lines. The water and the land regions in the feature space of TV and MB are marked accordingly in light blue and green, respectively.

have been labeled automatically as land. To avoid false classification in the case of a small dataset of backscatter observations, pixels with less than 10 backscatter measurements have been discarded. In this study, only the westernmost edge of the Andalusia study area could not be classified, corresponding to 5% of the total number of pixels in the study area.

A. Assessment of Water Body Mapping Accuracy

Verification of the water body maps obtained from the ASAR data is provided in the form of percentages of agreement with respect to (i) the CLC2006 product re-coded to water and non-water, or the SWBD product if the former was not available, and (ii) the samples extracted from Google Earth imagery. The wetland classes “marshes”, “peat bogs” and “salines” of the CLC2006 dataset were re-coded as land. The wetland class “inter-tidal flats” was re-coded as water in accordance with the definition of these in the GlobCover dataset. Regardless of the reference dataset, we use the terms of user’s and producer’s accuracy (UA and PA), overall accuracy (OA) and Kappa coefficient as defined in [48] to quantify the agreement between the SAR-based classification and a reference dataset. The UA estimates the error related to an inclusion of samples in a given class (commission error); conversely, the PA estimates the error related to an exclusion of sample units from a given class (omission error). The OA and the Kappa coefficient indicate the overall agreement between the SAR-based classification and the reference data. The latter statistic is used to detect a possible agreement by chance between two datasets, which is embedded in the definition of the OA. To assess the impact of shorelines on the percentages of agreement with respect to the raster datasets, both the original and the one-pixel edge-eroded version were used.

VI. CLASSIFICATION RESULTS AND DISCUSSION

The classification algorithm was applied to the SAR data processed at 300 m for each of the study areas. To assess the robustness of the mapping algorithm to seasonal conditions and particular land-cover characteristics, three different definitions for MB were tested: (i) the lowest backscatter, (ii) the backscatter

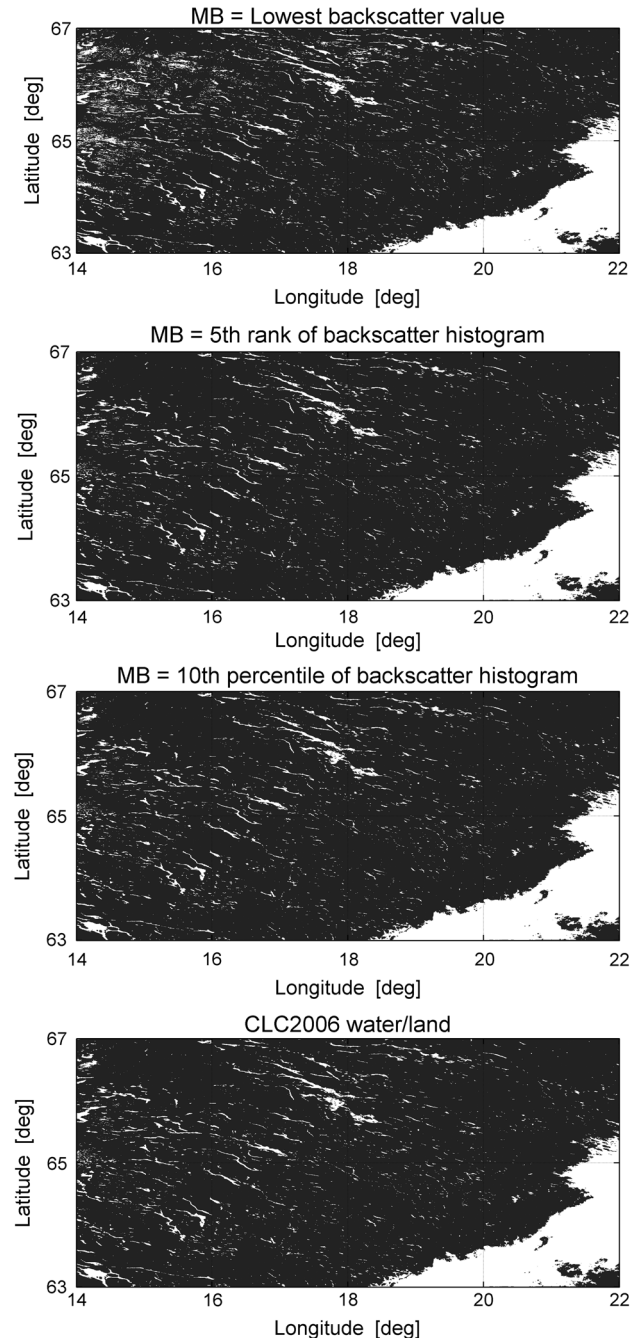


Fig. 14. ASAR-based water body maps using as MB the lowest backscatter value, the backscatter fifth rank and the backscatter 10th percentile. For reference, the CLC2006 dataset expressed in terms of a water and a land class is shown in the bottom panel. Grey is used for land, white is used for water. Study area: Västerbotten. Pixel size: 300 m \times 300 m. Note the larger amount of water bodies detected between 14°E and 16°E in the top panel with respect to the other panels.

fifth rank, and (iii) the backscatter 10th percentile. While using the rank as MB is more adequate for large backscatter datasets, the percentile is better suited when the multi-temporal dataset is small. The choice of definitions for the MB is not exhaustive; however, it was not the scope of this analysis to investigate the optimal selection of the MB channel. With (ii) and (iii), the aim was to demonstrate possible approaches to avoid that measurement noise and sporadic events would affect the MB value to cause false detections.

TABLE III

USER'S AND PRODUCER'S ACCURACY (UA AND PA), OVERALL ACCURACY (OA) AND KAPPA COEFFICIENT WITH RESPECT TO THE CLC2006 DATASET RECODED TO WATER AND LAND CLASSES OR THE SWBD PRODUCT, DEPENDING ON AVAILABILITY. THE SHADED ROWS REFER TO FIGURES RELATIVE TO THE ONE-PIXEL EDGE-ERODED VERSION OF EACH PRODUCT. ACCURACIES ARE REPORTED FOR THE MAP OBTAINED USING AS MB (i) THE LOWEST BACKSCATTER, (ii) THE BACKSCATTER FIFTH RANK AND (iii) THE BACKSCATTER 10TH PERCENTILE. PIXEL SIZE: 300 m × 300 m. ACCURACIES ARE IN THE FORM OF % VALUES

Study area (reference dataset)		UA water	UA land	PA water	PA land	OA	Kappa
Andalusia (CLC2006)	(i)	71.4	99.5	35.2	99.8	99.3	0.47
	(ii)	80.4	99.4	28.3	99.9	99.3	0.42
	(iii)	79.3	99.4	31.0	99.9	99.3	0.44
	(i)	77.6	99.9	80.8	99.9	99.8	0.79
	(ii)	90.3	99.9	71.5	100.0	99.9	0.80
	(iii)	89.6	100.0	78.1	100.0	99.9	0.83
Central Siberia (SWBD)	(i)	87.6	99.8	77.1	99.9	99.7	0.82
	(ii)	95.1	99.6	62.6	100.0	99.6	0.75
	(iii)	95.8	99.7	72.3	100.0	99.7	0.82
	(i)	82.8	100.0	99.3	99.9	99.9	0.90
	(ii)	93.5	99.9	88.4	100.0	99.9	0.91
	(iii)	94.2	100.0	98.5	100.0	99.9	0.96
Netherlands (CLC2006)	(i)	96.7	98.5	83.0	99.7	98.3	0.88
	(ii)	98.3	98.3	80.3	99.9	98.3	0.87
	(iii)	98.4	98.2	79.8	99.9	98.2	0.87
	(i)	98.1	99.8	98.8	99.7	99.5	0.98
	(ii)	99.5	99.7	98.0	99.9	99.6	0.98
	(iii)	99.5	99.6	97.8	99.9	99.6	0.98
Poland (CLC2006)	(i)	89.0	98.7	49.0	99.8	98.6	0.63
	(ii)	98.3	98.6	43.7	100.0	98.6	0.60
	(iii)	98.9	98.6	42.4	100.0	98.6	0.59
	(i)	90.6	99.9	96.6	99.7	99.6	0.93
	(ii)	99.0	99.9	95.4	100.0	99.8	0.97
	(iii)	99.6	99.9	94.9	100.0	99.8	0.97
Switzerland (SWBD)	(i)	85.6	99.6	80.3	99.7	99.3	0.83
	(ii)	95.9	99.5	77.3	99.9	99.5	0.85
	(iii)	93.6	99.6	78.8	99.9	99.4	0.85
	(i)	83.1	100.0	98.8	99.7	99.7	0.90
	(ii)	95.9	100.0	77.3	99.3	99.5	0.96
	(iii)	92.4	100.0	98.3	99.9	99.9	0.95
Västerbotten (CLC2006)	(i)	70.2	96.9	59.9	98.0	95.3	0.62
	(ii)	94.1	96.3	51.5	99.7	96.2	0.65
	(iii)	94.8	96.3	50.5	99.8	96.2	0.64
	(i)	74.1	99.7	95.9	97.3	97.1	0.82
	(ii)	95.9	99.4	92.7	99.7	99.1	0.93
	(iii)	96.1	99.4	92.8	99.7	99.2	0.94

A comparison of water body maps with respect to the reference dataset (CLC2006 re-coded to water and land) is shown in Fig. 14 for the study area of Västerbotten. Major water bodies and the Baltic Sea were mapped correctly regardless of the definition of MB. The MB set equal to the lowest backscatter value (Fig. 14, top panel) caused false detections of land surfaces as water in correspondence of the western edge of the study area between 14°E and 16°E. Here, wet snow conditions caused high TV and low MB when all measurements were considered (see also Fig. 2). Using a low-order parameter of the backscatter histogram rather than the absolute minimum implied that such special conditions were disregarded and the corresponding water body map (Fig. 14, central panels) presented stronger agreement with the reference (Fig. 14, bottom panel).

Table III reports agreement statistics for each of the six study areas when using the raster datasets (CLC2006 or SWBD) as reference. For study areas where both datasets were available, we note that the difference between accuracies using one or the other dataset was less than a few percent units. Table IV reports the agreement numbers in the case of the Google Earth samples with pure land and pure water information.

Mapping of water bodies performed better when using as MB a low-order parameter of the backscatter histogram (cf. UA of rows (ii) and (iii) with respect to the corresponding UAs

on row (i) in Table III). The commission error for the water class decreased because false detection of land as water could be avoided by neglecting data acquired under special environmental conditions that could distort the MB (Table III). The agreement statistics for the UA of the water class however did not give a clear indication on which of the two definitions here chosen for the MB metric (5th rank or 10th percentile) should ultimately be preferred (Tables III and IV). For classification based on a histogram parameter, the UA was above 92% for all study areas (rows (ii) and (iii) in Tables III and IV) except for Andalusia. The lower agreement was a consequence of a large portion of salines (wetlands) being detected as water. Because of the fragmentation of salines, the UA in the case of pure pixels was higher than when all pixels were considered (90% vs. 80%). Herewith, we note that wetlands in the form of marshes and peat bogs were detected as land in at least 95% of the cases. Intertidal flats were detected as water in more than 99% of the cases.

Mixed pixels, i.e., pixels along shorelines, were often labeled as land while they were defined as water in the reference dataset. Omissions of water areas were more frequent in study areas characterized by narrow water bodies (Andalusia, Poland, and Västerbotten). The PA of water was mostly in the 30% to 50% range (Table III). When shoreline pixels were excluded from the analysis, the PA of water was mostly above the 90% level

TABLE IV

USER'S AND PRODUCER'S ACCURACY (UA AND PA), OVERALL ACCURACY (OA) AND KAPPA COEFFICIENT WITH RESPECT TO GOOGLE EARTH SAMPLES (N = number of samples). THE VALIDATION DATASET CONSISTED OF POLYGONS WITH WATER FRACTION OF 100% (WATER CLASS) AND $< 10\%$ (LAND CLASS). ACCURACIES ARE REPORTED FOR THE MAP OBTAINED USING AS MB (i) THE LOWEST BACKSCATTER, (ii) THE BACKSCATTER FIFTH RANK AND (iii) THE BACKSCATTER 10TH PERCENTILE. PIXEL SIZE: 300 m \times 300 m. ACCURACIES ARE IN THE FORM OF % VALUES.

Study area		UA water	UA land	PA water	PA land	OA	Kappa
Andalusia N=192	(i)	93.9	97.5	88.6	98.7	96.9	0.89
	(ii)	100.0	96.9	85.7	100.0	97.4	0.91
	(iii)	100.0	97.5	88.6	100.0	97.9	0.93
Central Siberia N=179	(i)	100.0	98.5	99.1	100.0	99.4	0.99
	(ii)	100.0	86.1	90.1	100.0	93.8	0.87
	(iii)	100.0	97.1	98.2	100.0	98.9	0.98
Netherlands N=191	(i)	99.1	98.6	99.1	98.6	98.9	0.98
	(ii)	100.0	96.0	97.2	100.0	98.3	0.97
	(iii)	100.0	96.0	97.2	100.0	98.3	0.96
Poland N=178	(i)	100.0	99.2	98.2	100.0	99.4	0.99
	(ii)	100.0	99.2	98.2	100.0	99.4	0.99
	(iii)	100.0	97.6	94.6	100.0	98.3	0.96
Switzerland N=205	(i)	100.0	93.1	96.3	100.0	97.6	0.95
	(ii)	100.0	87.2	92.7	100.0	95.1	0.89
	(iii)	100.0	89.5	94.2	100.0	96.1	0.91
Västerbotten N=177	(i)	96.1	94.0	92.5	96.9	94.9	0.90
	(ii)	98.6	91.4	88.7	99.0	94.3	0.88
	(iii)	98.6	88.9	85.0	99.0	92.7	0.85

except for Andalusia where PA was between 71% and 81% depending on the definition of MB. The poorer performance of the mapping algorithm in Andalusia was related to the irregular shoreline of several water reservoirs which appeared smaller compared to the reference dataset. This indication is supported by the higher PA based on Google Earth samples (above 85%, Table IV), where the proportion of samples in correspondence of a shoreline was smaller compared to the CLC2006 dataset.

The overall classification accuracy was above 90% for all study areas (Tables III and IV). The Kappa coefficient instead depended on the definition used for MB and whether shoreline pixels had been excluded from the reference dataset (Table III). This in turn implied that size and shape of water bodies affected the Kappa coefficient. The lowest coefficients were obtained in Andalusia (45% and 80%, average of the three MB cases). For Poland and Västerbotten, the Kappa coefficient was of the order of 60% when shorelines were taken into account whereas for the remaining study areas the coefficient was approximately 80% (average of the three MB cases). When restricting to pure pixels only, the Kappa coefficient was above 90%.

To further quantify the impact of water fraction in a pixel on the accuracy of the water body maps, we illustrate in Fig. 15 the agreement statistics with respect to a threshold on water fraction in the case of the Netherlands study area. The PA of the water class and thus the UA of land improved for increasing minimum water fraction within a pixel because the omission of water areas was stronger in mixed pixels with larger fraction of land. Commission errors of water areas were very seldom (UA of water almost 100%) because in the case of mixed pixels, the multi-temporal metrics were found to be affected primarily by the properties of the radar backscatter from the land fraction within the pixel (see Section IV-C).

The OAs for the six study areas presented similar trends, indicating increased agreement between ASAR-based water body maps and reference datasets for threshold on water fraction (Fig. 16). Defining as water a pixel with at least 75% water fraction implied an overall mapping accuracy of approximately

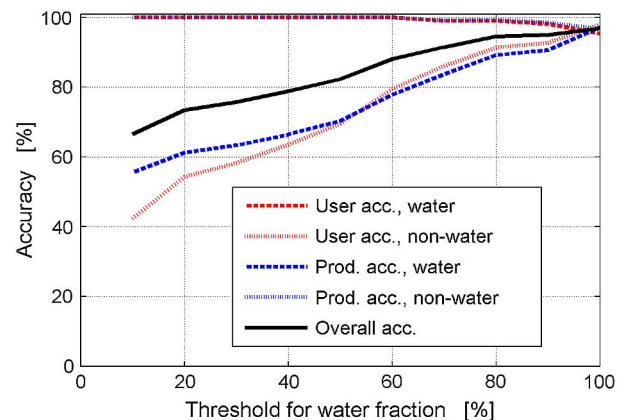


Fig. 15. UAs, PAs and OA with respect to a threshold for water fraction for the study area of the Netherlands. Pixel size: 300 m \times 300 m.

90%. A threshold of 50% was instead characterized by OAs between 75% and 85%. The differences of OA for a given threshold were related to the amount of water pixels omitted by the classification algorithm. Lower OAs were obtained for study areas with small water bodies and irregular shorelines.

The classification algorithm applied to SAR data with the pixel size of 150 m mapped features with a size on the order of 300 m which were omitted in the classification using the SAR data with the alike pixel size. As an example, in correspondence of the Rhine river delta in the study area of the Netherlands, the percentage of pixels labeled as water increased from 14.7% to 15.4%. To assess the impact of pixel size on the classification, we compared the agreement statistics between the ASAR-based water body maps and the reference datasets at 150 m and 300 m in Table V. When restricting to pure pixels of water and land (CLC2006 dataset), all agreement statistics were above 95% and the Kappa coefficient was above 0.97. Lower PA of water and in turn lower OA (approximately 88%) occurred when shoreline pixels were included in the reference dataset. Benchmarking against the Google Earth dataset indicated more omissions of

TABLE V

USER'S AND PRODUCER'S ACCURACY (UA AND PA), OVERALL ACCURACY (OA) AND KAPPA COEFFICIENT FOR THE 150 M PIXEL SIZE WITH RESPECT TO THE 300 M PIXEL SIZE (SHADED CELLS) FOR DIFFERENT REFERENCE DATASETS. THE MB CORRESPONDED TO THE BACKSCATTER FIFTH RANK. ACCURACIES ARE IN THE FORM OF % VALUES.

Reference dataset	UA water	UA land	PA water	PA land	OA	Kappa
Google Earth polygons (pure pixels)	100.0	88.0	90.8	100.0	94.5	0.89
	100.0	96.0	97.2	100.0	98.3	0.97
CLC2006 eroded	99.0	99.4	95.1	99.9	99.3	0.97
	99.5	99.7	98.0	99.9	99.6	0.98
CLC2006	98.0	98.4	82.4	99.8	98.4	0.89
	98.3	98.3	80.3	99.9	98.3	0.87

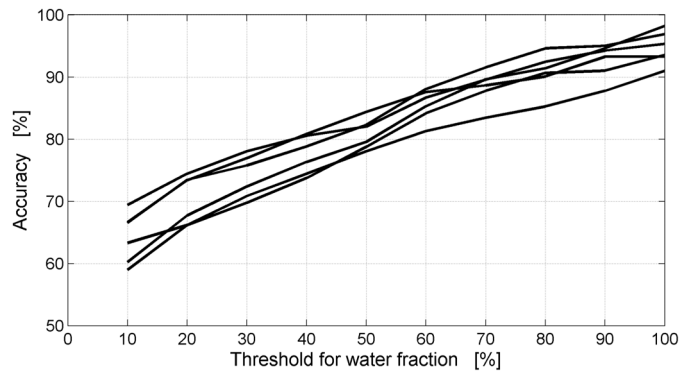


Fig. 16. OA for each study area with respect to the threshold for water fraction. Pixel size: 300 m \times 300 m.

water areas for the pixel size of 150 m than 300 m. At 300 m, several narrow-sized water bodies neither appeared in the reference dataset nor were detected in the ASAR data. Conversely, at 150 m they were still not detected in the ASAR data but appeared in the reference dataset although they were mostly characterized by a certain land fraction which in turn caused the omissions.

VII. CONCLUSIONS AND OUTLOOK

In this study, we looked at the potential of SAR multi-temporal metrics for land cover characterization with particular regard to discriminate between open water bodies and land surfaces. The SAR dataset consisted of C-band Envisat ASAR Wide Swath Mode images because of the large amount of data available worldwide, easy access and the moderate spatial resolution. Although data from other spaceborne SAR sensors might be more suitable for such application (e.g., L-band, dual-and full polarimetric data, shallow look angles, meter resolution), none satisfies the requirements of easy access, frequent and large-area coverage.

A simple thresholding algorithm based on the temporal variability (TV) of the SAR backscatter and the minimum backscatter (MB) estimated from stacks including at least 10 measurements could discriminate between permanent water bodies and land surfaces at 150 and 300 m pixel size in a consistent manner. Defining the MB as low order ranks or percentiles rather than the lowest backscatter served to avoid commission errors for the water class. The overall classification accuracy was above 90% when restricting to pure pixels; the accuracy decreased linearly with water fraction when also

mixed pixels were taken into account. For a threshold of 50% of water fraction, the overall accuracy was approximately 80%.

Omissions of water areas occurred in correspondence of mixed pixels with a water fraction and for narrow water bodies with irregular shorelines. Water bodies with a dimension less than twice the pixel size of the SAR data were not detected. High resolution images such as those provided by the forthcoming Sentinel-1 mission might reduce the area affected by omissions of water, particularly in the case of small-sized water bodies; it is however expected that mixed water/land pixels along shorelines are classified mostly as land since because the TV and MB are affected by the scattering properties of the objects within the resolution cell rather than by the resolution of the sensor itself.

While this study focused on mapping permanent water bodies, the approach presented here is in theory applicable also to monitor the dynamics of water bodies by using SAR data from selected time windows. Assessing the detection of water surfaces in consequence of temporary events like inundation and flooding would require dense time series of measurements in correspondence of the specific event. The availability of daily observations of ASAR Wide Swath Mode observations at latitudes north 60°N could be used to demonstrate the capability of time series of short-term TV and MB to track water dynamics in tundra regions.

ACKNOWLEDGMENT

P. Defourny, S. Bontemps, and J. Radoux, UCL, are acknowledged for advice on the classification approach. The SAR dataset was obtained through ESA's Category 1 Project ID 8073. K. Traut, FSU Jena, is acknowledged for support in the selection and the ordering of the Envisat ASAR data. The authors are truly indebted to the anonymous reviewers for their comments.

REFERENCES

- [1] S. Quegan and J. J. Yu, "Filtering of multichannel SAR images," *IEEE Trans. Geosci. Remote Sens.*, vol. 39, pp. 2373–2379, 2001.
- [2] C. Pathe, W. Wagner, D. Sabel, M. Doubkova, and J. B. Basara, "Using ENVISAT ASAR global mode data for surface soil moisture retrieval over Oklahoma, USA," *IEEE Trans. Geosci. Remote Sens.*, vol. 47, pp. 468–480, 2009.
- [3] A. Bartsch, W. Wagner, K. Scipal, C. Pathe, D. Sabel, and P. Wolski, "Global monitoring of wetlands—The value of ENVISAT ASAR global mode," *J. Environ. Manage.*, vol. 90, pp. 2226–2233, 2009.
- [4] B. Marti-Cardona, C. Lopez-Martinez, J. Dolz-Ripolles, and E. Bladè-Castellet, "ASAR polarimetric, multi-incidence angle and multitemporal characterization of Doñana wetlands for flood extent monitoring," *Remote Sens. Environ.*, vol. 114, pp. 2802–2815, 2010.

- [5] J. Reschke, A. Bartsch, S. Schlaffer, and D. Schepaschenko, "Capability of C-band SAR for operational wetland monitoring at high latitudes," *Remote Sens.*, vol. 4, pp. 2923–2943, 2012.
- [6] A. Bouvet and T. Le Toan, "Use of ENVISAT/ASAR wide-swath data for timely rice fields mapping in the Mekong River delta," *Remote Sens. Environ.*, vol. 115, pp. 1090–1101, 2011.
- [7] T. Geldsetzer, J. van der Sanden, and B. Brisco, "Monitoring lake ice during spring melt using RADARSAT-2 SAR," *Can. J. Remote Sens.*, vol. 36(S2), pp. 391–400, 2010.
- [8] A. Bartsch, A. M. Trofaier, G. Hayman, D. Sabel, S. Schlaffer, D. B. Clark, and E. Blyth, "Detection of open water dynamics with ENVISAT ASAR in support of land surface modelling at high latitudes," *Biogeosciences*, vol. 9, pp. 703–714, 2012.
- [9] C. Kuenzer, H. Guo, J. Huth, P. Leinenkugel, X. Li, and S. Dech, "Flood mapping and flood dynamics of the Mekong Delta: ENVISAT-ASAR-WSM based time series analyses," *Remote Sens.*, vol. 5, pp. 687–715, 2013.
- [10] S. Quegan, T. Le Toan, J. J. Yu, F. Ribbes, and N. Floury, "Multi-temporal ERS SAR analysis applied to forest mapping," *IEEE Trans. Geosci. Remote Sens.*, vol. 38, pp. 741–753, 2000.
- [11] U. Wegmüller, A. Wiesmann, T. Strozzi, and C. Werner, "Forest mapping with multi-temporal SAR," presented at the ForestSAT 2002 Conf., Edinburgh, U.K., Aug. 5–9, 2002.
- [12] P. Ahtonen and M. Hallikainen, "Automatic detection of water bodies from spaceborne SAR images," presented at the IGARSS'05, Seoul, Korea, Jul. 25–29, 2005.
- [13] A. Bartsch, C. Pathe, K. Scipal, and W. Wagner, "Detection of permanent open water surfaces in central Siberia with ENVISAT ASAR wide swath data with special emphasis on the estimation of methane fluxes from tundra wetlands," *Hydrol. Res.*, vol. 39.2, pp. 89–100, 2008.
- [14] B. Brisco, N. Short, J. van der Sanden, R. Landry, and D. Raymond, "A semi-automated tool for surface water mapping," *Can. J. Remote Sens.*, vol. 35, pp. 336–344, 2009.
- [15] T. Hahmann, S. Martinis, A. Twele, and M. Buchroithner, "Strategies for the automatic mapping of flooded areas and other water bodies from high resolution TerraSAR-X data," in *Cartography and Geoinformatics for Early Warning and Emergency Management: Towards Better Solutions*. Brno: Masaryk University, 2009, pp. 207–214.
- [16] M. Silveira, "Separation between water and land in SAR images using region-based level sets," *IEEE Geosci. Remote Sens. Lett.*, vol. 6, pp. 471–475, 2009.
- [17] V. Gstaiger, S. Gebhardt, J. Huth, T. Wehrmann, and C. Kuenzer, "Multi-sensoral derivation of inundated areas using TerraSAR-X and ENVISAT ASAR data," *Int. J. Remote Sens.*, vol. 33, pp. 7291–7304, 2012.
- [18] T. Hahmann and B. Wessel, "Surface water body detection in high-resolution TerraSAR-X data using active contour models," presented at the EUSAR 2010 Conf., Aachen, Germany, Jun. 7–10, 2010.
- [19] A. Wendleder, B. Wessel, A. Roth, M. Breunig, K. Martin, and S. Wagenbrenner, "TanDEM-X water indication mask: Generation and first evaluation results," *IEEE J. Sel. Topics Appl. Earth Observ. Remote Sens.*, vol. 6, pp. 171–179, 2013.
- [20] K. D. Unterschultz, J. van der Sanden, and F. E. Hicks, "Potential of RADARSAT-1 for the monitoring of river ice: Results of a case study on the Athabasca River at Fort McMurray, Canada," *Cold Regions Sci. Technol.*, vol. 55, pp. 238–248, 2009.
- [21] M. O. Jeffries, K. Morris, W. F. Weeks, and H. Wakabayashi, "Structural and stratigraphic features and ERS-1 synthetic aperture radar backscatter characteristics of ice growing on shallow lakes in NW Alaska, winter 1991–1992," *J. Geophys. Res.*, vol. 99, pp. 22459–22471, 1994.
- [22] C. R. Duguay, T. J. Pultz, P. M. Lafleur, and D. Drai, "RADARSAT backscatter characteristics of ice growing on shallow sub-Arctic lakes, Churchill, Manitoba, Canada," *Hydrol. Process.*, vol. 16, pp. 1631–1644, 2002.
- [23] M. Nolan, G. Liston, P. Prokein, J. Brigham-Grette, V. L. Sharpton, and R. Huntzinger, "Analysis of lake ice dynamics and morphology on Lake El'gygytgyn, NE Siberia, using synthetic aperture radar (SAR) and Landsat," *J. Geophys. Res.*, vol. 108, 2003.
- [24] T. Hirose, M. Kapfer, J. Bennett, P. Cott, G. Manson, and S. Solomon, "Bottomfast ice mapping and the measurement of ice thickness on tundra lakes using C-band synthetic aperture radar remote sensing," *J. Amer. Water Res. Assoc.*, vol. 44, pp. 285–292, 2008.
- [25] P. Bicheron, P. Defourny, C. Brockmann, L. Schouten, C. Vancutsem, M. Huc, S. Bontemps, M. Leroy, F. Achard, M. Herold, F. Ranera, and O. Arino, "GLOBCOVER—Products description and validation report," Media France 2008.
- [26] "ASAR product handbook," ESA ESRIN, no. 2.2, Feb. 27, 2007.
- [27] J. Closa, B. Rosich, and A. Monti Guarnieri, "The ASAR wide swath mode products," presented at the IGARSS'03, Toulouse, France, Jul. 21–25, 2003.
- [28] M. A. Friedl, D. K. McIver, J. C. F. Hodges, X. Y. Zhang, D. Muchoney, A. H. Strahler, C. E. Woodcock, S. Gopal, A. Schneider, A. Cooper, A. Baccini, F. Gao, and C. Schaaf, "Global land cover mapping from MODIS: Algorithms and early results," *Remote Sens. Environ.*, vol. 83, pp. 287–302, 2002.
- [29] U. Wegmüller, "Automated terrain corrected SAR geocoding," presented at the IGARSS'99, Hamburg, Germany, 28 Jun.–2 Jul. 1999.
- [30] B. Rabus, M. Eineder, A. Roth, and R. Bamler, "The shuttle radar topography mission—A new class of digital elevation models acquired by spaceborne SAR," *ISPRS J. Photogramm. Remote Sens.*, vol. 57, pp. 241–262, 2003.
- [31] J. de Ferranti, "Digital Elevation Data," 2009 [Online]. Available: <http://www.viewfinderpanoramas.org/dem3.html>
- [32] U. Wegmüller, C. Werner, T. Strozzi, and A. Wiesmann, "Automated and precise image registration procedures," in *Analysis of Multi-temporal Remote Sensing Images*, ser. Remote Sensing, Bruzzone and Smits, Eds. Trento, Italy: World Scientific, Sep. 13–14, 2001, vol. 2, pp. 37–49, 2002.
- [33] A. Lopes, E. Nezry, R. Touzi, and H. Laur, "Structure detection and statistical adaptive speckle filtering in SAR images," *Int. J. Remote Sens.*, vol. 14, pp. 1735–1758, 1993.
- [34] C. Oliver and S. Quegan, *Understanding Synthetic Aperture Radar Images*. Boston, MA, USA: Artech House, 1998.
- [35] A. Wiesmann, U. Wegmüller, M. Santoro, T. Strozzi, and C. Werner, "Multi-temporal and multi-incidence angle ASAR wide swath data for land cover information," in *Proc. 4th Int. Symp. Retrieval of Bio- and Geophysical Parameters from SAR Data for Land Applications*, Innsbruck, Austria, Nov. 16–19, 2004.
- [36] M. Santoro, C. Beer, O. Cartus, C. Schmullius, A. Shvidenko, I. McCallum, U. Wegmüller, and A. Wiesmann, "Retrieval of growing stock volume in boreal forest using hyper-temporal series of Envisat ASAR ScanSAR backscatter measurements," *Remote Sens. Environ.*, vol. 115, pp. 490–507, 2011.
- [37] G. Büttner, J. Feranec, G. Jaffrain, L. Man, G. Maucha, and T. Soukup, "The CORINE LAND COVER 2000 Project," *EARSel eProceedings*, vol. 3, pp. 331–346, 2004.
- [38] "Shuttle radar topography mission water body data set 2005," SWBD, Feb. 2012 [Online]. Available: <http://www2.jpl.nasa.gov/srtm/index.html>
- [39] "CLC2006 technical guidelines," European Environment Agency, EEA, Copenhagen, Denmark, 2007.
- [40] M. E. Ginevan, "Testing land-use map accuracy: Another look," *Photogramm. Eng. Remote Sens.*, vol. 45, pp. 1371–1377, 1979.
- [41] Envisat [Online]. Available: <https://directory.eoportal.org/web/eoportal/satellite-missions/e/envisat>
- [42] P. H. Swain and S. M. Davis, *Remote Sensing: The Quantitative Approach*. New York, NY, USA: McGraw-Hill, 1978.
- [43] T. Castel, A. Beaudoin, N. Stach, N. Stussi, T. Le Toan, and P. Durand, "Sensitivity of space-borne SAR data to forest parameters over sloping terrain. Theory and experiment," *Int. J. Remote Sens.*, vol. 22, pp. 2351–2376, 2001.
- [44] M. A. Tanase, M. Santoro, J. de la Riva, F. Pérez-Cabello, and T. Le Toan, "Sensitivity of X-, C- and L-band SAR backscatter to burn severity in Mediterranean pine forests," *IEEE Trans. Geosci. Remote Sens.*, vol. 48, pp. 3663–3675, 2010.
- [45] P. Defourny and S. Bontemps, "Revisiting land-cover mapping concepts," in *Remote Sensing of Land Use and Land Cover: Principles and Applications*, C. Giri, Ed. Boca Raton, FL, USA: CRC Press, 2012.
- [46] H. Stephen and D. G. Long, "Microwave backscatter modeling of ERG surfaces in the Sahara desert," *IEEE Trans. Geosci. Remote Sens.*, vol. 43, pp. 238–247, 2005.
- [47] W. G. Rees, *Remote Sensing of Snow and Ice*. Boca Raton, FL, USA: CRC Press, 2006.
- [48] R. G. Congalton, "A review of assessing the accuracy of classifications of remotely sensed data," *Remote Sens. Environ.*, vol. 37, pp. 35–46, 1991.



Maurizio Santoro (M'04) received the M.S. degree in aerospace engineering from the University of Naples "Federico II," Naples, Italy, in 1998, the Lic.Eng. degree from the Chalmers University of Technology, Gothenburg, Sweden, in 2001, and the Ph.D. degree from Friedrich-Schiller University, Jena, Germany, in 2003.

From 2004 to 2005, he held a postdoctoral position with Friedrich-Schiller University. Since 2006, he has been a Project Scientist with GAMMA Remote Sensing AG, Gümligen, Switzerland. His main duties include synthetic aperture radar (SAR) and interferometric SAR data processing and applications of SAR interferometry for land cover mapping. He is involved as Principal and Coinvestigator in several international projects on the use of Earth observation data for land cover mapping and monitoring. His main research interests include characterization of land cover using SAR and interferometric SAR data and retrieval techniques of forest biophysical parameters from SAR data.



Urs Wegmüller (M'94–SM'03) received the M.S. and Ph.D. degrees in physics from the University of Bern, Bern, Switzerland, in 1986 and 1990, respectively.

Between 1991 and 1992, he was with the Jet Propulsion Laboratory, California Institute of Technology, Pasadena, CA, USA. Between 1993 and 1995, he was with the University of Zürich, Zürich, Switzerland. In 1995, he was a Founding Member of GAMMA Remote Sensing AG (GAMMA), Gümligen, Switzerland, a Swiss company active in the development of signal processing techniques and remote sensing applications. As Chief Executive Officer of GAMMA, he has overall responsibility for GAMMA's activities. He is/was the Principal Investigator for projects supported by the European Space Agency and European Commission framework programs. At present, his main involvement is in the development of applications and the definition and implementation of related services in land surface deformation mapping, hazard mapping, land use mapping, and topographic mapping.